

Glueball mass measurements from improved staggered fermion simulations

Christopher M. Richards, Alan C. Irving
*Theoretical Physics Division, Department of Mathematical Sciences,
 University of Liverpool, Liverpool L69-7ZL, United Kingdom*

Eric B. Gregory
Department of Physics, University of Cyprus, P.O. Box 20357 1678 Nicosia, Cyprus

Craig McNeile
Bergische Universität Wuppertal, Gausstr. 20, D-42119 Wuppertal, Germany

(UKQCD collaboration)
 (Dated: May 14, 2010)

We present the first 2+1 flavour spectrum measurements of glueball states using high statistics simulations with improved staggered fermions. We find a spectrum consistent with quenched measurements of scalar, pseudoscalar and tensor glueball states. The measurements were made using 5000 configurations at a lattice spacing of 0.123 fm and pion mass of 280 MeV and 3000 configurations at 0.092 fm with a pion mass of 360 MeV. We see some evidence of coupling to 2π states. We compare our results with the experimental glueball candidate spectrum as well as quenched glueball estimates.

PACS numbers: 11.15.Ha, 12.38.Gc, 14.40.Be

I. INTRODUCTION

During the last decade, a major first-principles calculation of the hadron spectrum has been carried out based on the improved staggered fermion discretisation formalism [1, 2]. Comparisons with experiment, have in most cases shown impressive agreement, typically within a few percent accuracy. See for example [3] and references therein and a recent review article by the MILC collaboration [4]. Noticeably absent from this impressive list are some singlet quantities such as those contributing to glueball states and to the η/η' system. Since the latter states are stable under the strong interaction, they may be classified as ‘gold-plated’ quantities [3] and so deserve urgent consideration as a test of this otherwise highly successful formalism. This is made all the more pressing in view of the continuing controversy over the validity of the so-called ‘fourth-root trick’ for dealing with the spurious taste multiplicity. See [5] for a comprehensive review of this. A major difficulty in simulating singlet quantities is the need to make high quality stochastic estimates of disconnected correlators which are typically very noisy observables. In dynamical simulations the problem is particularly severe due to the high simulation costs. An analysis of these measurement problems and initial results using MILC configurations [6] has recently been presented [7]. We have now completed significantly higher statistics simulations at two lattice spacings primarily in order to study the η/η' . (These results will be presented elsewhere.) As a by-product, we have also made measurements of scalar meson operators and glueball operators. The latter form the basis of the present paper.

In the quenched approximation, comprehensive studies of the glueball spectrum have been available for some time [8–10]. In comparison, studies with dynamical quarks are still at a preliminary stage [11–14]. This is mainly because glue correlators are noisy and the masses relatively high so that signal to noise is hard to control without large statistics. The quenched studies typically used thousands of configurations rather than the ‘few hundred’ configurations usually available at a given lattice spacing and quark mass. We therefore took the opportunity to make use of several thousand configurations generated as part of the main singlet simulation program. Preliminary results were presented in [14].

Crede and Meyer [15] and Klempt and Zaitsev [16] have recently reviewed the past and future experimental searches for glueballs. It is particularly timely to study the glueball spectrum using unquenched QCD, because there are new experiments starting, or starting soon, that are looking for glueballs. The BES-III experiment [17] has begun running and can search for glueballs via radiative J/ψ decays. It will study light mesons with 0^{-+} , 2^{++} , and 0^{++} quantum numbers, where glueball degrees of freedom could contribute.

It will be particularly interesting to see if the existence of $f_J(2220)$ as a state is confirmed by BES-III [17]. The $f_J(2220)$ is a candidate 2^{++} state that some speculate is a glueball state because its mass is close to the mass of the 2^{++} glueball, (2390(30)(120) MeV, in the quenched estimates of Chen et al. [10]. The 120 MeV error is from different ways of setting the lattice spacing in quenched QCD, parametrised by uncertainty in r_0 . Recently the HPQCD determined r_0 to 0.8% accuracy from unquenched lattice QCD [18]. Using HPQCD’s central value of $1/r_0 = 423$ MeV, changes

the mass of the 2^{++} glueball to 2470(30) MeV. This shift is within the errors of the quenched estimate [10], but illustrates the need for unquenched calculations.

The PANDA experiment at FAIR will look for glueballs in the range 2.2 to 5.5 GeV [19, 20] after 2015.

The general plan of the paper is as follows. In section II we describe the simulations, the ensembles and the methods used for extracting spectrum information. The next section III contains the results from these calculations. The paper ends with a discussion of these results and some conclusions in section IV.

II. SIMULATION AND MEASUREMENTS

A. Configuration ensembles

Available resources allowed us to produce an initial two ensembles corresponding to existing MILC ensembles, but with significantly greater statistics and making use of an exact algorithm, the RHMC [21, 22] rather than the R algorithm. The simulation parameters are summarised in Table I.

ensemble	N_f	β	$L^3 \times T$	am_l/s	r_0/a	a [fm]	N_{cfg}	N_{traj}
coarse	2+1	6.75	$24^3 \times 64$	0.006/0.03	3.8122(74)	0.12250(24)	5237	31422
fine	2+1	7.095	$32^3 \times 64$	0.00775/0.031	5.059(10)	0.09230(19)	2867	17202

TABLE I: Ensembles generated for flavour singlet studies.

We used an improved version of the RHMC algorithm [22] which made use of such things as the ‘ n^{th} -root trick’, higher order integrators and different types of mass-preconditioning. Additional parameters to be tuned included gauge/fermion step sizes and the conjugate gradient tolerance used in different parts of the force calculation and acceptance tests. Details of the tuning procedures and other properties of the simulations are given in [23].

The lattice spacing was determined via the static potential using standard methods [24]. When required, the value of r_0 used to convert to physical scales was 0.467 fm.¹

The ‘coarse’ ensemble summarised in Table I represents some 8 times the statistics of the corresponding $20^3 \times 64$ MILC configuration studied in [7] while the fine ensemble represents an increase of around 5 on a typical MILC ensemble. We have studied the autocorrelation time for simple operators. For technical reasons the first simulations (coarse ensemble) which were conducted on the UKQCD QCDOC machine [25] were interrupted at various times resulting in non-contiguous RHMC trajectories. The ensemble was produced in two separate streams. The fine lattice simulations however resulted in an uninterrupted Markov chain, so allowing investigation of some autocorrelations. Table II shows the integrated autocorrelation times of some relevant observables which can be meaningfully defined on a single configuration. The effective masses (defined below) are those using both local (L) and fuzzed(F) sources

	LL	LF	FF
m_{eff}^π	2.28(33)	2.29(32)	1.99(21)
	$i = 0$	$i = 1$	$i = 2$
$\mathcal{P}_i^{A_1^{++}}(0)$	0.65(6)	0.89(21)	1.12(9)
$\sum_t \mathcal{P}_i^{A_1^{++}}(t)$	1.13(15)	1.61(22)	2.59(26)

TABLE II: Integrated autocorrelation times (in units of 6 trajectories) for the effective mass of the pion (averaged over euclidean times 8 – 10) and for the plaquette based glue operators-defined below for a fixed time plane ($t = 0$) and also averaged over all time planes.

and sinks for the $\gamma_5 \times \gamma_5$ pion operator. The glue operators are defined in the next section. The labels $i = 0, 1, 2$ refer to the number of Teper blocking levels as described below. As expected, the pion shows a longer autocorrelation than a single time plane operator. We have not detected any evidence of autocorrelation in the glueball correlators and corresponding effective masses which, as discussed below, are very noisy. We have checked, by binning in selected cases, that the statistical error estimates made using configurations separated by 6 trajectories are reasonable.

¹ A recent accurate determination by the HPQCD collaboration using MILC ensembles gave $r_0 = 0.4661(38)$ [18]

The coarse ensemble has been successfully incorporated by the MILC collaboration into an analysis of the strange quark content of the nucleon [26].

B. Glueball measurement methods

We used standard glue operators $\mathcal{P}^{A_1^{++}}$ built from spatial plaquettes for the O_h irrep A_1^{++} (coupling to 0^{++} in the continuum). Prior to measurement we use APE smearing [27] (twice with smearing parameter $c = 2.5$) and then Teper blocking [28] performed n times where $n = 0, 1, 2, \dots, N-1$. Using all N blocking levels provides an N -dimensional basis for the variational measurement techniques as described below. The APE smearing smooths out some of the ultra-violet noise while the different Teper blocking levels provide a basis of operators with a range of physical extents allowing different couplings to the ground state and excited states in a given channel. This is important when using variationally motivated techniques as outlined below. We also use these plaquette operators $\mathcal{P}^{\mathcal{R}}$ for the E_1^{++} and T_2^{++} irreps (\mathcal{R}) which couple to 2^{++} states in the continuum. For example, for E_1^{++} we use both the operators in (1) (standard) and (2) (alternative).

$$\mathcal{P}_i^{E_1^{++}}(t) = \text{tr} \sum_{\vec{x}} (P_{4,xy}^i(\vec{x}, t) - P_{4,yz}^i(\vec{x}, t)) \quad (1)$$

and

$$\mathcal{P}_i'^{E_1^{++}}(t) = \text{tr} \sum_{\vec{x}} (P_{4,xy}^i(\vec{x}, t) + P_{4,yz}^i - 2P_{4,zx}^i(\vec{x}, t)) . \quad (2)$$

For pseudoscalar operators (A_1^{-+}) we require something non-planar with some ‘handedness’ [29]. In practice, see (3), we use left (L) and right (R) handed versions of the loop shown in Fig 1.

$$\begin{aligned} \mathcal{H}_i^{A_1^{-+}}(t) = \text{tr} \sum_{\vec{x}} & \left((H_{8,L,xy}^i(t) + H_{8,L,yz}^i(t) + H_{8,L,zx}^i(t)) \right. \\ & \left. - (H_{8,R,xy}^i(t) + H_{8,R,yz}^i(t) + H_{8,R,zx}^i(t)) \right) . \end{aligned} \quad (3)$$

We refer to operators $\mathcal{H}^{\mathcal{R}}$ based on these as ‘hand’ operators in what follows.

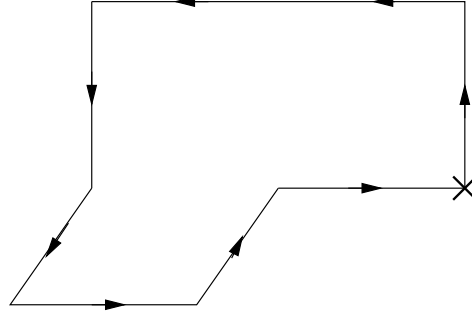


FIG. 1: Schematic of the (left) hand operator \mathcal{H}_0 which can be used to study the pseudoscalar glueball.

We calculate correlators (vacuum-subtracted where necessary) between operators with definite momentum on time planes separated by euclidean time t

$$C_{ij}^{\mathcal{R}}(t) = \langle \mathcal{O}_i^{\mathcal{R}}(0) \mathcal{O}_j^{\mathcal{R}}(t) \rangle . \quad (4)$$

Here \mathcal{R} refers to the O_h irrep under consideration and i, j refer to the operator basis being used e.g. different Teper blocking levels. These matrices of correlators form the basis of subsequent analyses as described below.

1. *Effective masses.* These are defined generically by

$$am_{\text{eff}} = \ln \frac{C(t)}{C(t+1)} . \quad (5)$$

where $C(t)$ is $C_{ij}^{\mathcal{R}}(t)$ for some choice of \mathcal{R} and $i = j$. Typically, a plateau in $am_{\text{eff}}(t)$ is observed at lower values of t when i corresponds to higher levels of blocking. Weighted averages over the plateau region can then be used to estimate the ground state mass in channel \mathcal{R} . When using an improved gauge action containing links over more than one time-plane, as here, one should be alert to possible positivity violations at small euclidean time [30]. However, we have not encountered any unusual behaviour in this regard.

2. *Variational methods.* In the basic variational method [31–33] one finds eigenvalues of the $N \times N$ matrix

$$M_{ij}^{\mathcal{R}}(t, t_0) \equiv \sum_{k=1}^N [C^{\mathcal{R}}(t_0)]_{ik}^{-1} C_{kj}^{\mathcal{R}}(t) \quad (6)$$

where t_0 is some initial euclidean time at which the correlator matrix is sufficiently well-determined to be invertible. It is straightforward to show (see for example the factorising fit parametrisation given below) that the eigenvalues $\lambda^\alpha(t_0, t)$ of $M^{\mathcal{R}}(t_0, t)$ are related to the transfer matrix and

$$\lambda^\alpha(t_0, t) = e^{-m_\alpha(t-t_0)} \quad (\alpha = 0, 1, \dots, N-1). \quad (7)$$

One can then either

- (a) use directly the masses am^α obtained from (7) or
- (b) form an effective mass, as in (5) above, from the ground state ($\alpha = 0$) projection of $C(t)$.

For convenience, we refer to masses estimated via (a) as ‘eigenvalue masses’ and those estimated via (b) as ‘variational effective masses’.

3. *Factorising fits.* Using the usual intermediate state arguments, the correlator matrix (4) can be expressed as an infinite sum of exponential contributions and fitted in truncated form so as to extract mass estimates:

$$C_{ij}(t) = \sum_{\alpha=0}^{M-1} c_i^\alpha c_j^\alpha e^{-m_\alpha t}. \quad (8)$$

Here we have suppressed the irrep label \mathcal{R} and restricted the sum to the M lowest-lying states. Note that by choosing $M = N$, the dimension of the operator basis, one can simply recover the variational formula given above. The factorised coefficient c_i^α gives the overlap of state α with operator i .

Note that in this study we have included only glue-based operator correlations in our factorising fits and corresponding variational analyses. In section III we will comment further on the prospects for studies of two meson operators and decay studies in general.

III. RESULTS

A. Results for the scalar glueball – coarse ensemble

We first give some sample results of the above methods applied to the coarse lattices. Fig. 2 shows the basic effective masses of the momentum 0 scalar state for each of the blocking levels 0 to 3. Despite the significantly larger statistics, compared with previous dynamical simulations, it is clear that the ratio of signal to noise is still a significant problem. Weighted averages of the ‘plateau’ values are shown for blocking levels 2 and 3. Here the weighting is inversely proportional to the statistical error. As with all other quantities in this study, overall statistical errors were estimated via bootstrap.

Fig. 3 shows the variational effective masses, as defined in section IIB (method 2b) deduced from a 3×3 correlator matrix (blocking levels 0 to 2)

Similar effective mass estimates were made using momentum 1 operators. The latter require no vacuum subtraction.

In Fig. 4 we show the lowest 3 masses (where obtainable) extracted from the variational matrix (method 2a). The momentum 1 masses have been obtained from energies using the naïve lattice dispersion relation. There is a reasonable degree of consistency with respect to the choice of t/t_0 except at large t where there is a suggestion that the lowest state projected out corresponds to a $\pi\pi$ system. Given that for these light quark masses, the two π decay threshold is open, this is not unexpected.

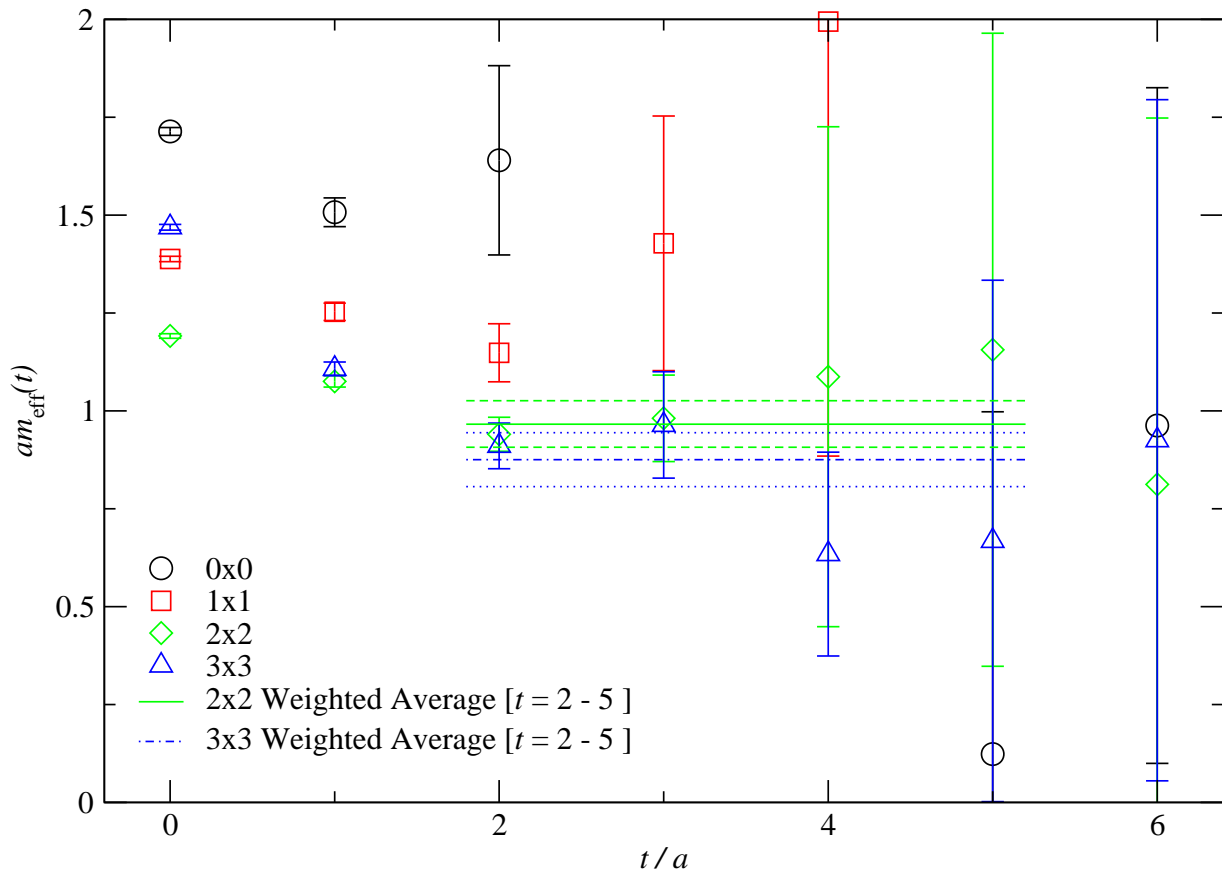


FIG. 2: The effective masses for the diagonal entries $(0,0)$, $(1,1)$ etc. of a 4×4 matrix of correlators formed using the $|p| = 0$ standard scalar operators with blocking levels 0 to 3 measured on the coarse ensemble. Weighted averages for blocking levels 2 and 3 are shown, computed from $t = 2 - 5$.

Similar studies were made using the alternative hand operators defined in section II B. The results were statistically consistent with those obtained from the standard operators. Fig. 5 shows a comparison of the lowest three states using standard and alternative operators.

Finally in this subsection, we present results of the third method: multichannel factorising fits. We have carried out 3×3 and 4×4 fits with 2 and 3 exponentials. We have studied both correlated and uncorrelated fits. We also investigated stability with respect to the fitted t range $t_{\min} \leq t \leq t_{\max}$. For example, Fig. 6 shows the variation with t_{\min} of the lowest two states resulting from two and three exponential fits to a 4×4 matrix of correlators (blocking levels 0 – 3). These fits are fully correlated and the corresponding fit details are listed in Table III.

The extent of consistency between the various methods can be judged from Fig. 7. The solid line, with dashed errors, represents a global average of these determinations. This average was obtained using the methods adopted by the Particle Data Group [34] when combining results from independent determinations. The errors used in the weighting are combined systematic and statistical errors. Of course, the statistical errors in our case are not independent. For each type of determination contributing to Fig. 7, represented by a central value and error bar, we have used the same weighted averaging procedure. The systematic errors took into account the variation due to fit range. In fact, the determinations contributing to the global average are a selected sub-group of all the various estimates and fits described above [23]. We have excluded fits which had unacceptably high (or low) $\chi^2/\text{d.o.f.}$ and/or which had very large errors, and also those which were found to have high sensitivity to fit ranges and/or parameter choices. Similar considerations were applied to the determination of the first excited state in the scalar sector, also shown in Fig. 7. We have only quoted fitted mass values for states where at least one higher state has been included in the determination. The global averages for the lowest two states in the scalar channel are shown in Table IV, along with the corresponding values for the fine lattices (described in the next subsection). We will return later to the physical interpretation of these results.

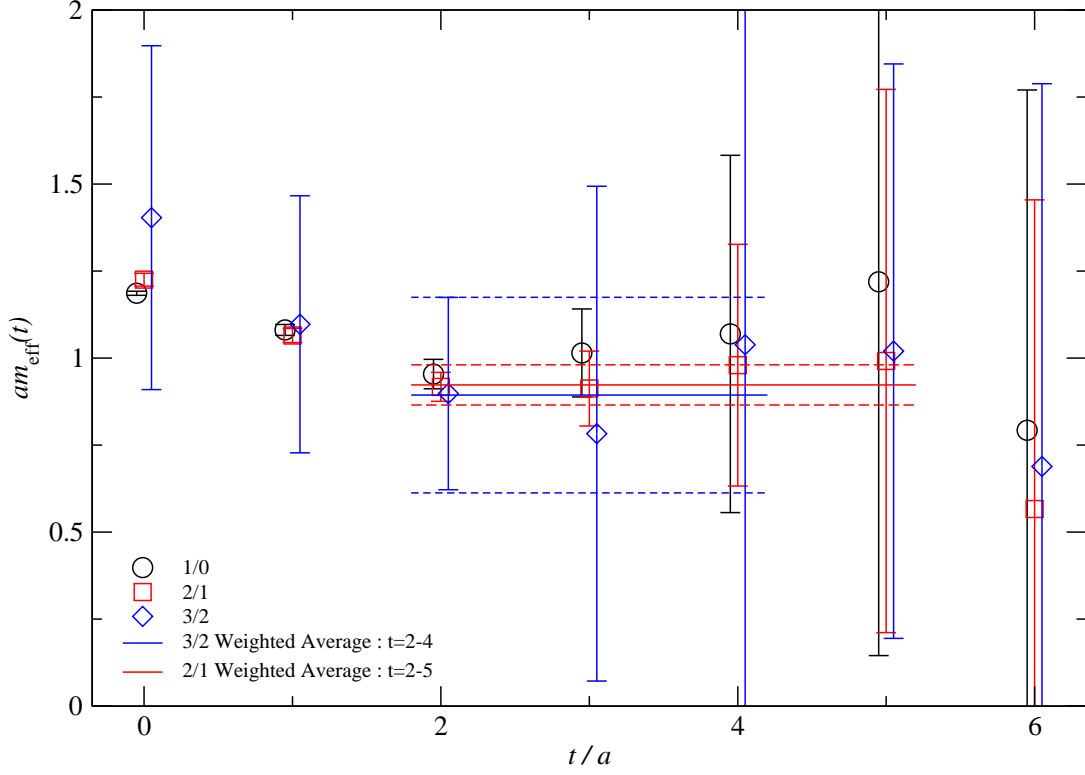


FIG. 3: Effective masses computed using the variational correlator for different choices of t/t_0 . Weighted averages are shown for the 2/1 and 3/2 projections (coarse ensemble, standard scalar glue operators).

N_{exp}	$ p $	t_{min}	t_{max}	am_0	am_1	am_2	$\chi^2/\text{d.o.f.}$
2	0	1	6	1.0336(29)	1.84(11)	—	3.176
		2	6	0.887(14)	1.332(47)	—	0.635
		3	6	0.62(13)	1.22(10)	—	0.349
2	1	1	6	1.0770(60)	1.70(14)	—	0.832
		2	6	1.034(36)	1.42(22)	—	0.301
		3	6	1.19(15)	3.30[—]	—	0.189
3	0	1	6	0.9409(43)	1.626(37)	18.04[—]	1.309
		2	6	0.32(15)	0.9495(57)	1.77[—]	0.607
		3	6	0.306(92)	1.016(17)	7.79[—]	0.327
3	1	1	6	1.0682(60)	1.623(75)	21.26[—]	0.329
		2	6	1.046(31)	1.41(20)	3.53[—]	0.173

TABLE III: Fitted mass parameters for two and three-exponential factorising fits to a 4×4 matrix of correlators using blocking levels 0 – 3 (coarse ensemble). Where errors are quoted as [—] this indicates that the gradient in that direction of parameter space was undetermined.

ensemble	a [fm]	am	am^*
coarse	0.12250(24)	1.0468(75)	1.875(87)
fine	0.09230(19)	0.8332(59)	1.368(17)

TABLE IV: Global average values for scalar masses on coarse and fine ensembles

B. Results for the scalar glueball – fine ensemble

Fig. 8 (corresponding to Fig. 3 for the coarse ensemble) shows variational effective scalar masses and weighted averages on the fine ensemble. In Fig. 9, we show the lowest 3 masses extracted from the variational matrix as described in method 2a. This is to be compared with Fig. 4 for the coarse ensemble, but in this case we take the

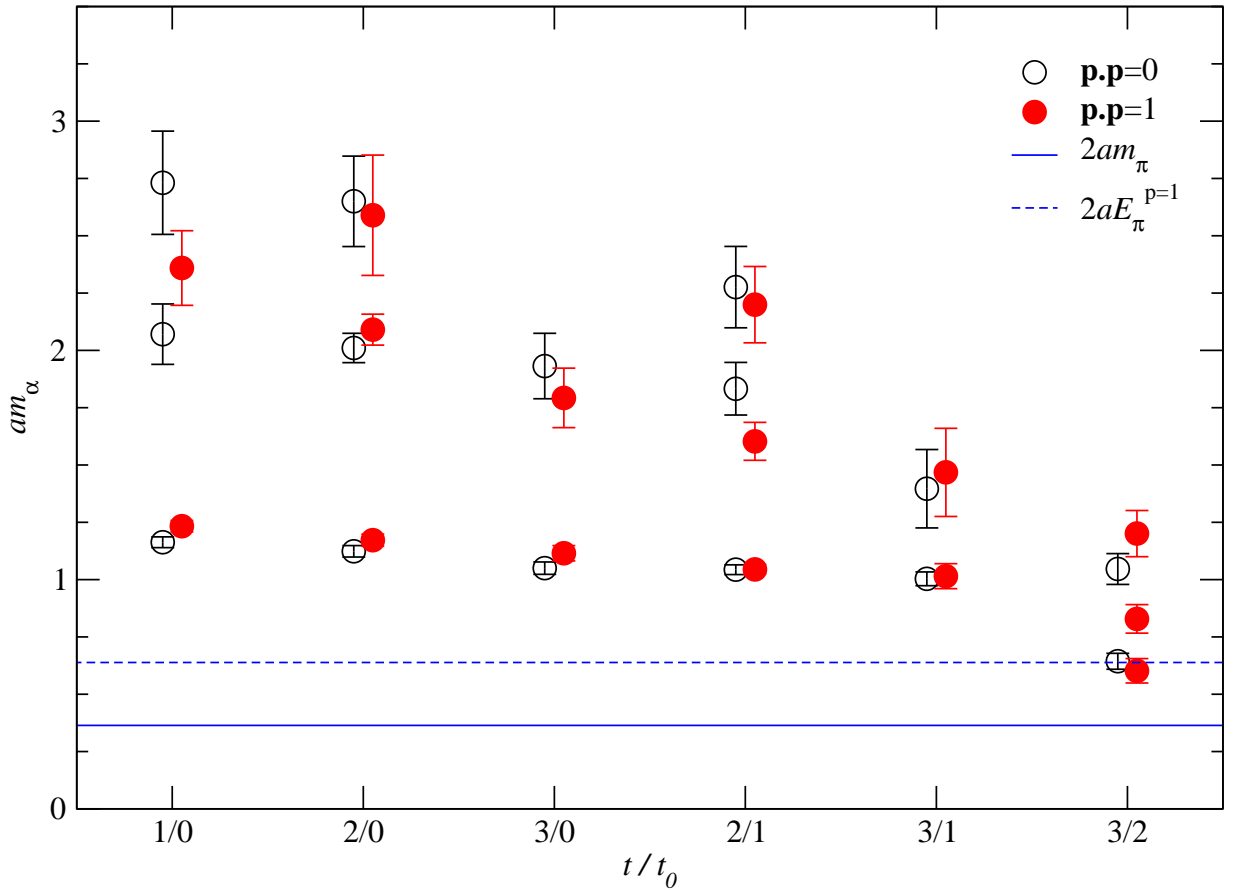


FIG. 4: The masses extracted from the variational eigenvalues for different t/t_0 using blocking levels 0, 2, 3 for momentum 0 and 1, 2, 3 for momentum 1. The energies corresponding to a $\pi\pi$ state with momentum 0 and 1 are drawn for comparison (coarse ensemble, standard scalar glue operators).

opportunity to display results for both standard and alternative (hand) operators. Both operator bases gave consistent results.

As examples of factorising fits on the fine ensemble, we present the t_{\max} dependence at fixed t_{\min} in Fig. 10. These are 4×4 fits using two and three exponentials. We see excellent consistency for the groundstates between the $M = 2$ (both $|p| = 0$ and 1) and the $M = 3$, $|p| = 1$ fits. The corresponding fit quality can be judged from Tables V and VI.

As with the coarse ensemble, we have selected the most reliable determinations for each of the described methods and assigned systematic errors to cover sensitivity to parameter and fit range. As an example, Fig. 11 shows sample variational results (effective mass and eigenvalue methods) for momentum zero and one. The relevant time slices t/t_0 are shown on the horizontal axis along with the t range used for averaging the effective mass.

The final values selected for all methods are shown in Fig. 12 along with the resulting global average using the same weighting procedures described earlier in section III A.

C. Scalar decay and mixing

Having observed signals in our fits which appear close to the 2π threshold, we have attempted to check the strength of mixing between the glueball and $\pi\pi$ operators. Early attempts to study the mixing directly have been made [35] but were performed at pion masses such that $2m_\pi$ was just below m_G . One might naively expect that glueball decay would be flavour blind, decaying into $\pi\pi$, $K\bar{K}$ and $\eta\eta$ final states with equal rates. Of course, since we are now observing the state (or states) to which the gluonic operators couple most strongly, then mixing effects are likely to violate flavour blindness. If the ‘glueball’ mixes strongly with a mainly $u\bar{u} + d\bar{d}$ state then the $\pi\pi$ decay channel is preferred over the OZI suppressed $K\bar{K}$ channel, and vice versa if the coupling is strongest to an $s\bar{s}$ state. There are

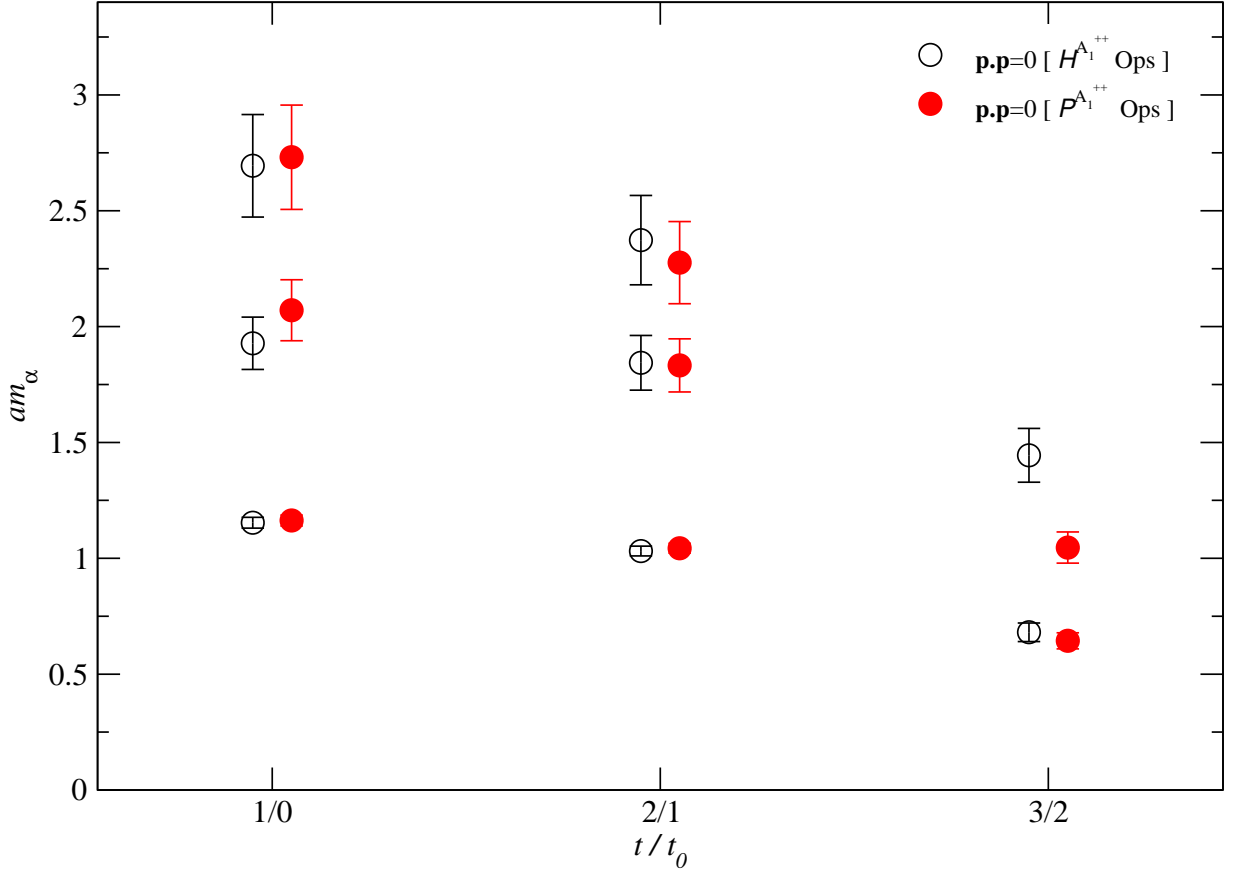


FIG. 5: The masses extracted from variational eigenvalues for different t/t_0 (coarse ensemble). These were made using blocking levels 0, 1, 2 for standard plaquette (filled circles) and alternative hand (empty circles) operators.

chiral suppression arguments [36] that suggest that $KK\bar{b}$ could dominate the two meson decay channel in a glueball state in this mass range.

One can in principle study decay matrix elements directly on the lattice following the procedure of Lellouch and Lüscher [37]. However this requires very accurate determinations on different lattice sizes and is a difficult technique to apply even for states which are much less subject to noise than those in the glueball sector. Initial attempts to study resonant states with open decay channels have been made - for example the PACS-CS collaboration [38] has studied the isovector P -wave phase shift in $\pi\pi$ scattering in order to estimate the width of the ρ meson. Additional complications and extra diagrams introduced in the case of staggered fermions have been detailed for example in [39] where $I = 2$ phase shifts were studied. In the isoscalar channel there are of course the further complications arising from disconnected contributions. The possible types of correlators required for a mixing study of glueball, f_0 and $\pi\pi$ are indicated in Fig. 13. Unquenched studies of mixing in the isoscalar 0^{++} system were carried out by Hart et al. [13] using two flavours of Wilson fermions. The ratio of diagram (i) to diagram (h) (see Fig. 13) was estimated using all to all techniques with 100 configurations. Unfortunately the errors were too large to provide useful information within the statistics of that study.

It has become clear that techniques for studying lattice decays will best be developed first in simpler and less noisy systems than isoscalar channels such as the present one.

So, for a preliminary study with improved staggered fermions, we choose instead to follow a simplified version of the method of [40] and form the mixing matrix

$$M_{ab}(t) = \begin{pmatrix} M_{GG}(t) & M_{\pi G}(t) \\ M_{G\pi}(t) & M_{\pi\pi}(t) \end{pmatrix} = \begin{pmatrix} \langle \mathcal{P}_i^{A_1^{++}}(0) \mathcal{P}_i^{A_1^{++}}(t) \rangle & \langle C_\pi(0) \mathcal{P}_i^{A_1^{++}}(t) \rangle \\ \langle \mathcal{P}_i^{A_1^{++}}(t) C_\pi(0) \rangle & \langle C_\pi(t) C_\pi(t) \rangle \end{pmatrix} \quad (9)$$

where $\mathcal{P}_i^{A_1^{++}}(0)$ and $\mathcal{P}_i^{A_1^{++}}(t)$ are the $|\vec{p}| = 0$ standard scalar glueball operators at timeslices 0 and t respectively, and $C_\pi(0)$ and $C_\pi(t)$ are the single pion correlators on timeslice 0 and t respectively. The $C_\pi(0)$ correlator allows

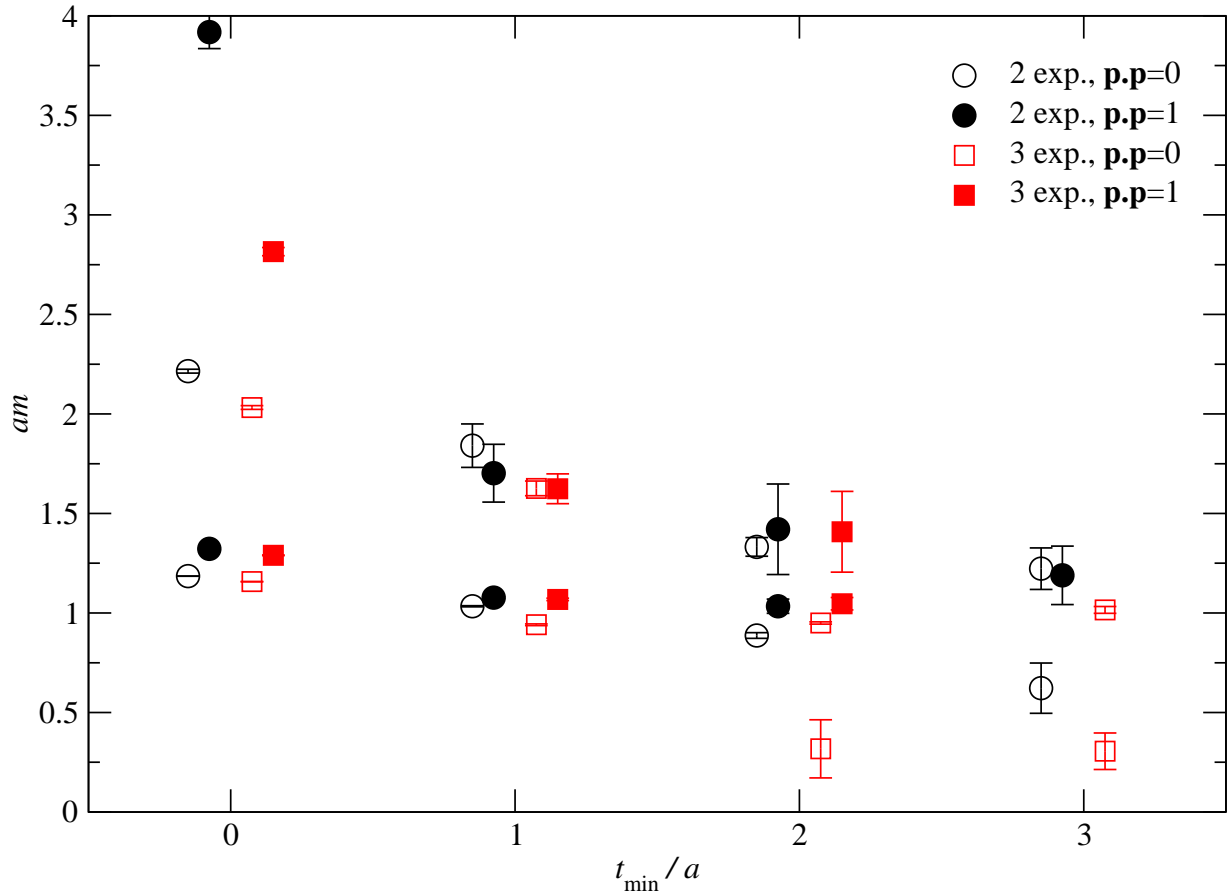


FIG. 6: Results from factorising fits applied to the 4×4 basis of standard scalar glueball operators with blocking levels 0 to 3. Both two and three-exponential fits are presented for momentum 0 and 1 correlators, with $t_{\max} = 6$ and t_{\min} allowed to vary (coarse ensemble).

us to study a $\pi\pi$ state localised in time and, because of the way we have computed the connected correlator, we are restricted to using $C_\pi(0)$ which reduces our statistics for the 2π operators by a factor of $n_t = 64$.

We form the ratio [40]

$$x_{G\pi}(t) = \frac{M_{G\pi}(t)}{\sqrt{M_{GG}(t)M_{\pi\pi}(t)}} \quad (10)$$

where the $M_{ab}(t)$ are the elements of (9) on timeslice t . This gives a measure of the off-diagonal mixing matrix elements, normalised by the diagonal entries. We remind the reader that this captures only some of the possible contractions contributing in a full treatment of the mixing as indicated in Fig. 13. In this study, the factorising fits involved diagrams of type (a) only and the estimated strength of mixing to $\pi\pi$ involved an approximation to (c).

We have computed these ratios for the coarse and fine lattices, using the glueball operator with three levels of Teper blocking (*i.e.* $\mathcal{P}_3^{A^{++}}$) which we found shows similar behaviour to the lower blocking levels but with less noise. We used the pion correlators with both local source and local sink, and fuzzed source and fuzzed sink. Our results are presented in Fig. 14.

For the coarse ratios we see that at small t they appear consistent with zero, turning negative for $t \sim 5$, although with large error. We note that the fine mixing ratio shows a similar downturn for $t \sim 3 - 4$. Whilst these ratios give only a guide to the mixing of the glueball operators and a $\pi\pi$ state, the small size of $x_{G\pi}$ at low t indicates that, provided we choose t_{\min} small enough, we should obtain a good overlap with the ‘stable’ glueball and conversely, that by choosing t_{\min} large, we may obtain a significant overlap with the $\pi\pi$ state. This is consistent with the earlier observations of the effective masses and factorising fits at small and large t .

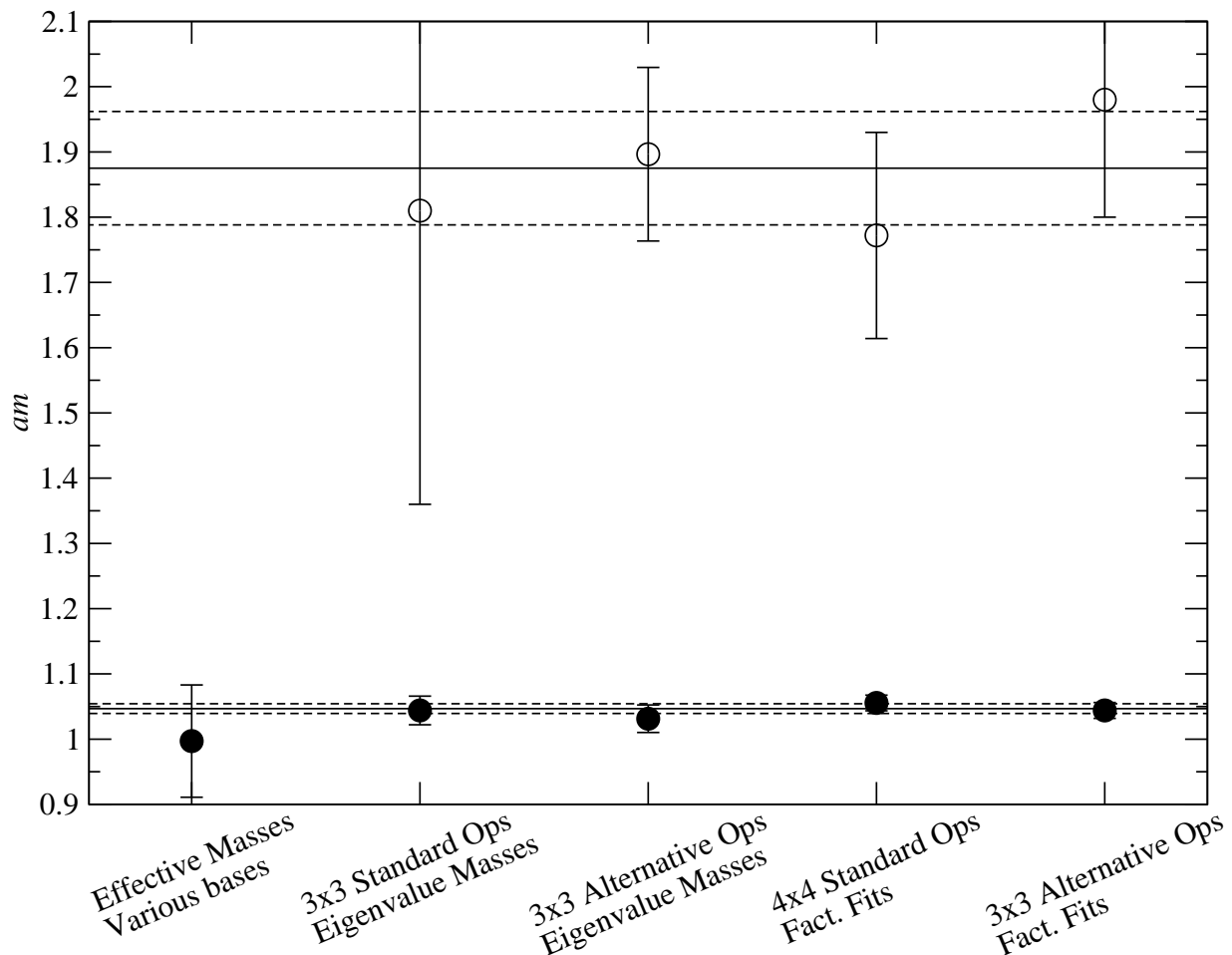


FIG. 7: The overall average for the scalar glueball groundstate and first excited state masses on the coarse ensemble, computed as described in the text.

D. Comparison with other scalar determinations

This study of scalar states in the glueball sector is characterised by relatively high statistics in comparison with previous studies using dynamical fermions. It also uses a vacuum with $2 + 1$ flavours. However, it is limited in that it makes use of only two lattice spacings (roughly 0.12 and 0.09 fm) and a single light quark mass for each ensemble. The pion mass in lattice units is 0.1740(6) (coarse ensemble) and 0.1672(14) (fine). These correspond to around 280 MeV and 360 MeV respectively so the quark masses are not particularly light. The strange quark mass is close to the physical one. Any attempt to extract a continuum limit (without a chiral limit of course) needs to be treated with due caution. In Table VII we summarise the scalar sector results in lattice units and in dimensionless form using the Sommer r_0 parameter from Table I.

In Fig. 15 we present our results along with those from a recent UKQCD study of scalar glueballs using staggered fermions (MILC configurations) [41], a UKQCD study using $\mathcal{O}(a)$ non-perturbatively improved Wilson fermions ($N_f = 2$) [11] and the continuum limit result from a quenched anisotropic study of the glueball spectrum [9]. We perform a simple continuum extrapolation using the form

$$r_0 m(a) = r_0 m_G + b(r_0/a)^4 \quad (11)$$

where $r_0 m_G$ and b are the parameters to be determined. In [9], this was found to work well for all glueball states except for the A_1^{++} where this was thought to be due to strong lattice spacing dependence caused by proximity to the non-physical phase transition in the Wilson fundamental-adjoint plane for the anisotropic lattice action used. However, the alternative form employed in [9] has four free parameters which we are unable to use with just two data points. As noted above, it is ambitious to attempt any kind of continuum extrapolation using two data points only and we emphasise that the fit with (11) has been performed as a guide only. Nevertheless, we that note good consistency

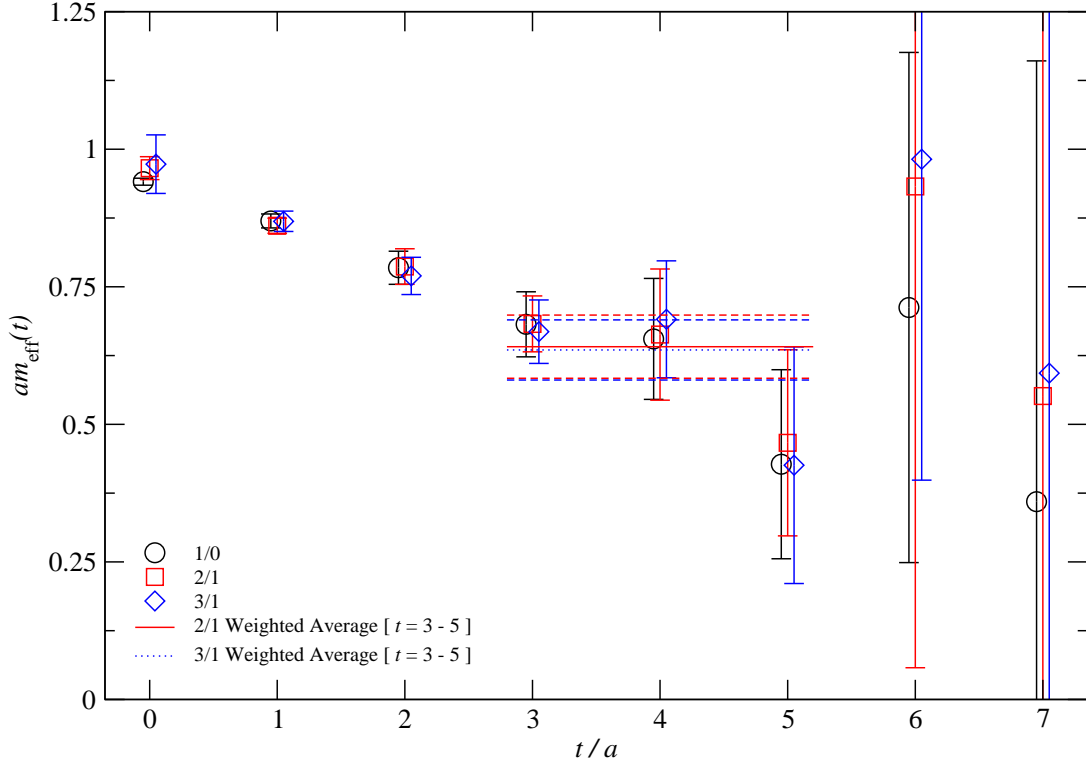


FIG. 8: Variational effective masses for the scalar glueball computed with different choices of t/t_0 , projecting from a 4×4 matrix (blocking levels 0, 1, 2, 3) measured on the fine lattices. Weighted averages are shown for the 2/1 and 3/1 projections.

N_{exp}	$ p $	t_{min}	t_{max}	am_0	am_1	am_2	$\chi^2/\text{d.o.f.}$
2	0	1	3	0.84139(97)	19.84[—]	—	7.233
		1	4	0.8237(17)	1.681(71)	—	5.098
		1	5	0.82[—]	1.73[—]	—	5.255
		1	6	0.84937(76)	692[—]	—	31.42
		1	7	0.81705(91)	19.16[—]	—	6.747
		1	8	0.81657(92)	19.06[—]	—	6.515
		1	9	0.80834(81)	1.77[—]	—	5.182
2	1	1	3	0.8521(15)	19.56[—]	—	8.185
		1	4	0.8528(13)	1.53[—]	—	3.604
		1	5	0.8517(12)	1.53[—]	—	2.885
		1	6	0.8985(14)	692[—]	—	37.12
		1	7	0.8446(13)	19.00[—]	—	3.838
		1	8	0.8446(13)	18.93[—]	—	3.368
		1	9	0.8480(11)	1.54[—]	—	1.933

TABLE V: Fitted mass parameters for two-exponential fully correlated factorising fits to a 4×4 matrix of correlators using a blocking levels 0, 1, 2, 3 with $|p| = 0$ and 1 for varying t_{max} with t_{min} fixed at $t = 1$ (fine ensemble). Where errors are quoted as [—] this indicates that the gradient in that direction of parameter space could not be determined.

between our continuum value for $r_0 m_G$ so obtained, 4.32(6), and the quenched value $r_0 m_G = 4.21(11)(4)$ [9]. Our extrapolated value corresponds to a physical value of 1.83 GeV approximately.

Our masses seem to show rather weak dependence on a — certainly weaker than that observed in [11] and of a similar strength to that observed in [9].

In Fig. 16 we present our results plotted against the pion mass, shown with the same comparisons from the literature as in Fig. 15. One might tentatively claim that the glueball mass increases as one decreases the pion mass, hinting at some underlying mixing dynamics. However the UKQCD measurements on the coarse MILC Asqtad ensembles are rather spread out and if, as is suspected, the $\mathcal{O}(a)$ improved Wilson measurements are suppressed by the phase structure of the action used [11] then they should probably be discounted and there remains very little trend to study.

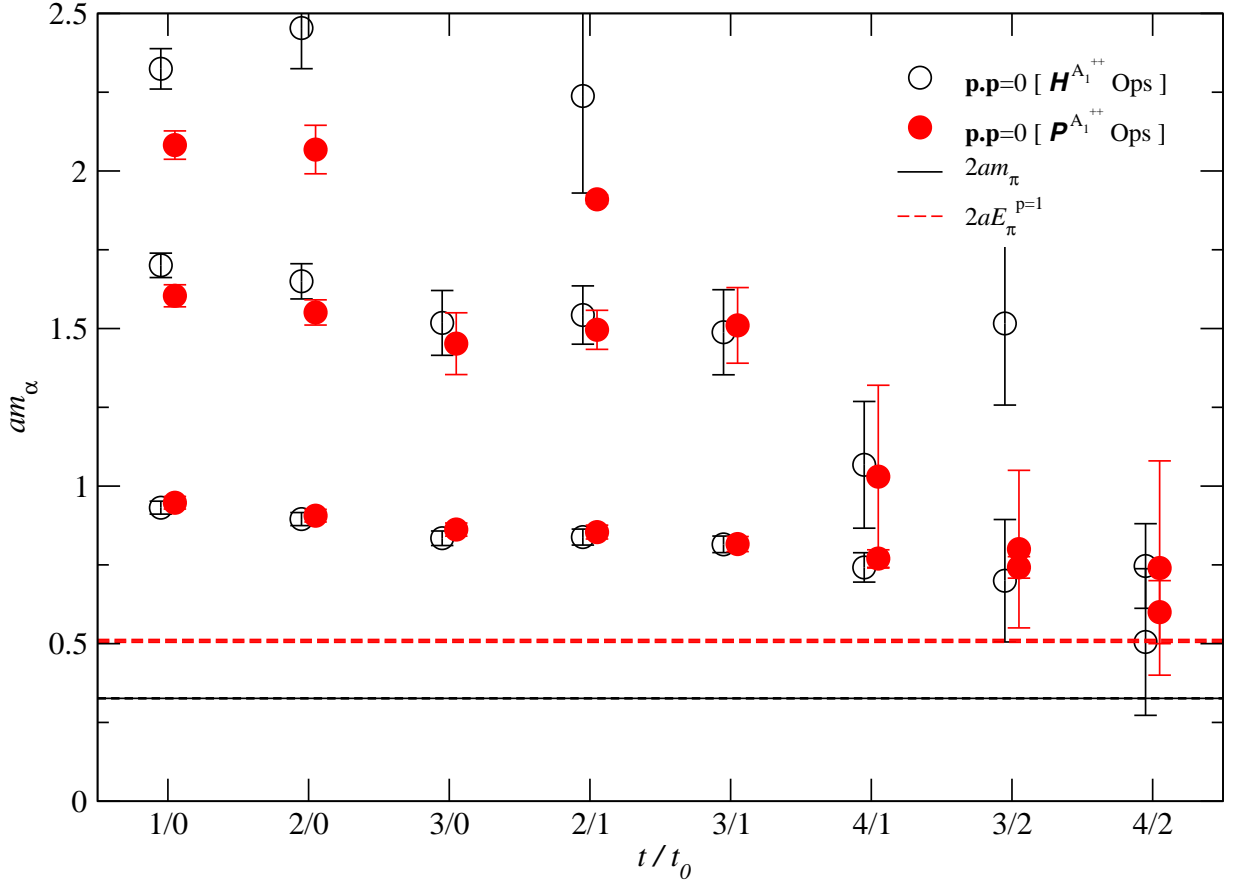


FIG. 9: Scalar glueball masses extracted, for the fine ensemble, from the variational eigenvalues using blocking levels 0, 1, 2 for different t/t_0 . Results based on the standard and alternative (hand) operators are compared. The energies corresponding to a $\pi\pi$ state with relative momenta $|p| = 0$ and $|p| = 1$ are drawn for comparison (fine ensemble).

E. Tensor and pseudoscalar glueball results

Similar procedures were used to obtain estimates of the ground state and first excited state in the pseudoscalar and tensor glueball channels. For the former we used blocked operators (3) based on the \mathcal{H} operators while for the latter we used those based on \mathcal{P} – see (1) and (2). Sample eigenvalue masses are shown in Fig. 17 and Fig. 18 for the pseudoscalar and tensor states respectively.

The global averages are given in Table VIII. For technical reasons, we were unable to complete measurements of the tensor state on the fine ensemble. For comparison, the quenched continuum limit estimates of $r_0 m$ from [9] are 6.33(13) and 5.85(8) for pseudoscalar and tensor glueballs respectively. So, just as for the scalar channel, there is little evidence of strong unquenching effects.

We have conducted a separate study of the η/η' system using connected and disconnected meson operators which will be presented elsewhere. Just for orientation, we note that the continuum (experimental) values of $r_0 m$ would be 1.32 (2.27) for the η (η') respectively. It is clear that there should be little mixing between the pseudoscalar glueball and the η' . However, further excited states in this singlet channel may mix.

There have been claims that the pseudoscalar $\eta(1405)$ meson [42, 43] contains significant mixtures of the pseudoscalar glueball. This requires that there is a significant shift of the mass of the pseudoscalar glueball between quenched and unquenched QCD, which we don't find in this calculation. However, note the qualifications accompanying our conclusions below.

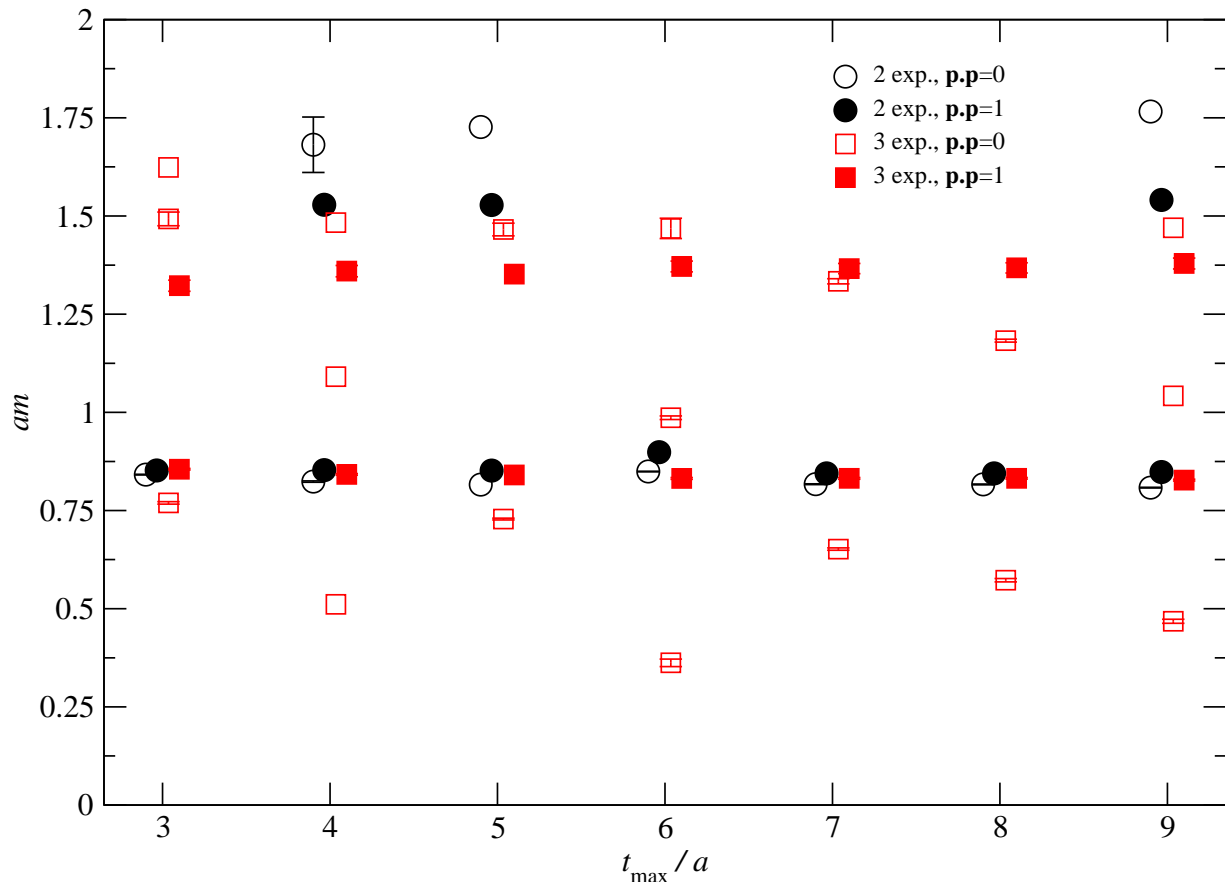


FIG. 10: Results from factorising fits applied to the 4×4 basis of standard scalar glueball operators (blocking levels 0, 1, 2, 3) measured on the fine lattices. Both two and three-exponential fits are presented for momentum 0, 1 correlators, with $t_{\min} = 1$ and t_{\max} allowed to vary.

IV. DISCUSSION AND CONCLUSIONS

We have presented the first high statistics study of the low-lying glueball sector in $2+1$ flavour QCD. We analysed some 5000 configurations of a $24^3 \times 64$ lattice with spacing 0.12 fm and 3000 configurations of a $32^3 \times 64$ lattice with spacing 0.09 fm using improved staggered (Asqtad) dynamical fermions. In contrast with earlier glueball analyses using improved Wilson fermions, we find no evidence of strong unquenching effects. For the 0^{++} , 0^{-+} and 2^{++} states we obtain mass estimates quite close to the continuum limit masses obtained in the quenched approximation [9]. In Fig. 19 we show a compilation of 0^{++} , 0^{-+} and 2^{++} glueball candidate states [34] together with quenched continuum limit predictions [9] and our unquenched results at fixed lattice spacing and fixed quark mass.

Despite the larger statistics available to us, we still had difficulty obtaining unambiguous estimates of even the low-lying states. This was due to at least two main factors - the inherently noisy correlators and the presence of open decay channels, particularly $\pi\pi$. In order to reduce the noise, we used a variety of smearing and blocking techniques giving access to a range of basis states. We also used a number of different methods based on variational techniques: effective masses, transfer matrix eigenvalues and multi-channel factorising fits. The effects of the open decay channels were exposed at larger euclidean time via the choice of fit ranges and also via direct evaluation of a subset of mixing matrix elements.

Our overall conclusions are:

- there is little evidence of large unquenching effects on the predicted low-lying glueball spectrum;
- accurate determination of masses requires even larger numbers of configurations in comparison with quenched glueball analyses;
- a fuller account must be taken of two meson state contributions at large euclidean time;

N_{exp}	$ p $	t_{min}	t_{max}	am_0	am_1	am_2	$\chi^2/\text{d.o.f.}$
3	0	1	3	0.7695(31)	1.493(17)	1.62[–]	1.549
		1	4	0.51[–]	1.09[–]	1.48[–]	1.450
		1	5	0.7284(22)	1.466(16)	20.29[–]	1.987
		1	6	0.3622(96)	0.9863(45)	1.468(26)	1.126
		1	7	0.6518(30)	1.3337(66)	16.65[–]	2.495
		1	8	0.5726(43)	1.1827(37)	19.78[–]	2.648
		1	9	0.4679(51)	1.04[–]	1.47[–]	1.866
3	1	1	3	0.8551(21)	1.322(14)	2.67(12)	0.144
		1	4	0.8420(21)	1.360(14)	2.73(20)	0.431
		1	5	0.84[–]	1.352(13)	22.23[–]	0.378
		1	6	0.8317(22)	1.371(14)	2.57[–]	0.542
		1	7	0.8319(20)	1.366(13)	18.17[–]	0.642
		1	8	0.8319(20)	1.368(13)	21.12[–]	0.585
		1	9	0.8274(23)	1.379(14)	2.40[–]	0.540

TABLE VI: Fitted mass parameters for three-exponential fully correlated factorising fits to a 4×4 matrix of correlators using a blocking levels 0, 1, 2, 3 with $|p| = 0$ and 1 for varying t_{max} with t_{min} fixed at $t = 1$ (fine ensemble).

Result	$am(A_1^{++})$	$r_0m(A_1^{++})$
Coarse – Ground	1.0468(75)	3.991(36)
Fine – Ground	0.8332(59)	4.215(38)
Coarse – Excited	1.875(87)	7.15(35)
Fine – Excited	1.368(17)	6.92(10)

TABLE VII: Scalar glueball masses (ground and first-excited states) from the coarse and fine lattices converted into units of the Sommer parameter r_0 .

- we encountered no problems that could be identified as resulting from the use of improved staggered fermions – in particular, the lattice spacing dependence was weak.

ACKNOWLEDGMENTS

We are grateful to Chris Michael for advice on fitting techniques and discussions on mixing. We acknowledge the use of the SCIDAC-funded Chroma package in this analysis [44].

-
- [1] MILC, K. Orginos and D. Toussaint, Phys. Rev. **D59**, 014501 (1998), hep-lat/9805009,
[2] C. Aubin *et al.*, Phys. Rev. **D70**, 094505 (2004), hep-lat/0402030,
[3] HPQCD, C. T. H. Davies *et al.*, Phys. Rev. Lett. **92**, 022001 (2004), hep-lat/0304004,
[4] A. Bazavov *et al.*, (2009), 0903.3598,
[5] S. R. Sharpe, PoS **LAT2006**, 022 (2006), hep-lat/0610094,
[6] C. W. Bernard *et al.*, Phys. Rev. **D64**, 054506 (2001), hep-lat/0104002,
[7] E. B. Gregory, A. C. Irving, C. M. Richards, and C. McNeile, Phys. Rev. **D77**, 065019 (2008), 0709.4224,
[8] UKQCD, G. S. Bali *et al.*, Phys. Lett. **B309**, 378 (1993), hep-lat/9304012,
[9] C. J. Morningstar and M. J. Peardon, Phys. Rev. **D60**, 034509 (1999), hep-lat/9901004,
[10] Y. Chen *et al.*, Phys. Rev. **D73**, 014516 (2006), hep-lat/0510074,
[11] UKQCD, A. Hart and M. Teper, Phys. Rev. **D65**, 034502 (2002), hep-lat/0108022,
[12] TXL, G. S. Bali *et al.*, Phys. Rev. **D62**, 054503 (2000), hep-lat/0003012,
[13] UKQCD, A. Hart, C. McNeile, C. Michael, and J. Pickavance, Phys. Rev. **D74**, 114504 (2006), hep-lat/0608026,
[14] UKQCD, E. B. Gregory, C. McNeile, A. C. Irving, and C. Richards, PoS **LATTICE2008**, 286 (2008), 0810.0136,
[15] V. Crede and C. A. Meyer, Prog. Part. Nucl. Phys. **63**, 74 (2009), 0812.0600,
[16] E. Klempt and A. Zaitsev, Phys. Rept. **454**, 1 (2007), 0708.4016,
[17] J.-M. Bian *et al.*, Int. J. Mod. Phys. **A24**, 173 (2009),
[18] HPQCD, C. T. H. Davies, E. Follana, I. D. Kendall, G. P. Lepage, and C. McNeile, Phys. Rev. **D81**, 034506 (2010), 0910.1229,
[19] PANDA, . M. F. M. Lutz, B. Pire, O. Scholten, and R. Timmermans, (2009), 0903.3905,
[20] PANDA, J. G. Messchendorp, (2010), 1001.0272,

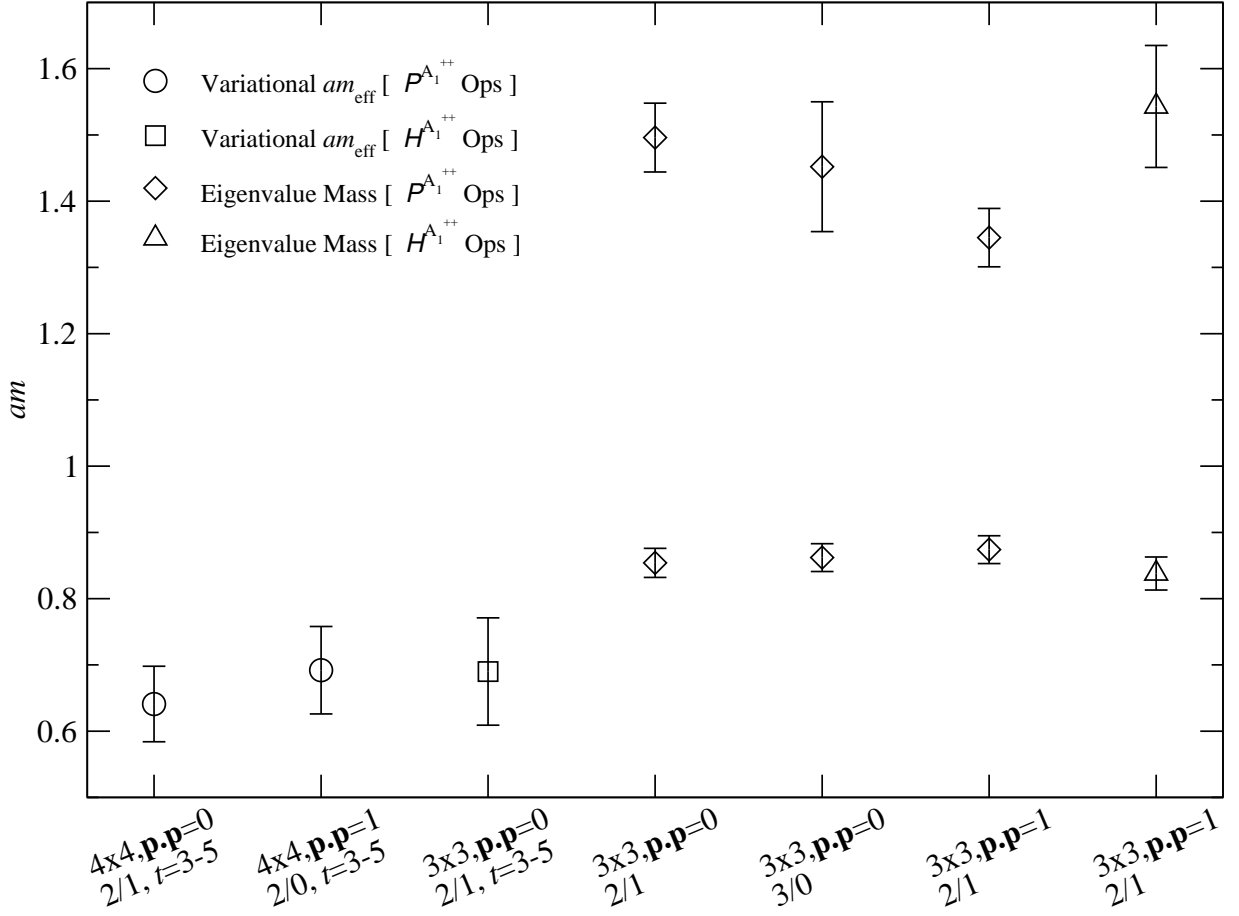


FIG. 11: Comparison of mass estimates obtained for the scalar glueball using different methods (variational effective masses and variational eigenvalues) for the fine ensemble. The points are described briefly on the axis and in the text.

Result	$am(A_1^{++})$	$r_0m(A_1^{++})$	$am(E_1^{++})$	$r_0m(E_1^{++})$
Coarse – Ground	1.560(67)	5.95(12)	1.510(13)	5.756(61)
Fine – Ground	1.265(17)	6.399(99)	–	–
Coarse – Excited	1.956(65)	7.46(26)	1.98(26)	7.55±1.01
Fine – Excited	1.984(77)	10.04(41)	–	–

TABLE VIII: Pseudoscalar and tensor glueball masses (ground and first-excited states) from the coarse and fine ensembles converted into units of the Sommer parameter r_0 . Pseudoscalar measurements were made on 3506/1998 configurations of the coarse/fine ensembles respectively. Tensor measurements were made on 2627 configurations of the coarse ensemble only.

- [21] M. A. Clark and A. D. Kennedy, Nucl. Phys. Proc. Suppl. **129**, 850 (2004), hep-lat/0309084,
- [22] M. A. Clark and A. D. Kennedy, Phys. Rev. **D75**, 011502 (2007), hep-lat/0610047,
- [23] C. M. Richards, *A high statistics study of the scalar singlet states in lattice QCD*, PhD thesis, University of Liverpool, 2009.
- [24] UKQCD, C. R. Allton *et al.*, Phys. Rev. **D65**, 054502 (2002), hep-lat/0107021,
- [25] P. Boyle *et al.*, Nucl. Phys. Proc. Suppl. **140**, 169 (2005),
- [26] MILC, D. Toussaint and W. Freeman, Phys. Rev. Lett. **103**, 122002 (2009), 0905.2432,
- [27] APE, M. Albanese *et al.*, Phys. Lett. **B192**, 163 (1987),
- [28] M. Teper, Phys. Lett. **B183**, 345 (1987),
- [29] B. Berg and A. Billoire, Nucl. Phys. **B221**, 109 (1983),
- [30] M. Luscher and P. Weisz, Nucl. Phys. **B240**, 349 (1984),
- [31] C. Michael and I. Teasdale, Nucl. Phys. **B215**, 433 (1983),
- [32] B. Blossier, M. Della Morte, G. von Hippel, T. Mendes, and R. Sommer, JHEP **04**, 094 (2009), 0902.1265,
- [33] S. Necco, Nucl. Phys. **B683**, 137 (2004), hep-lat/0309017,

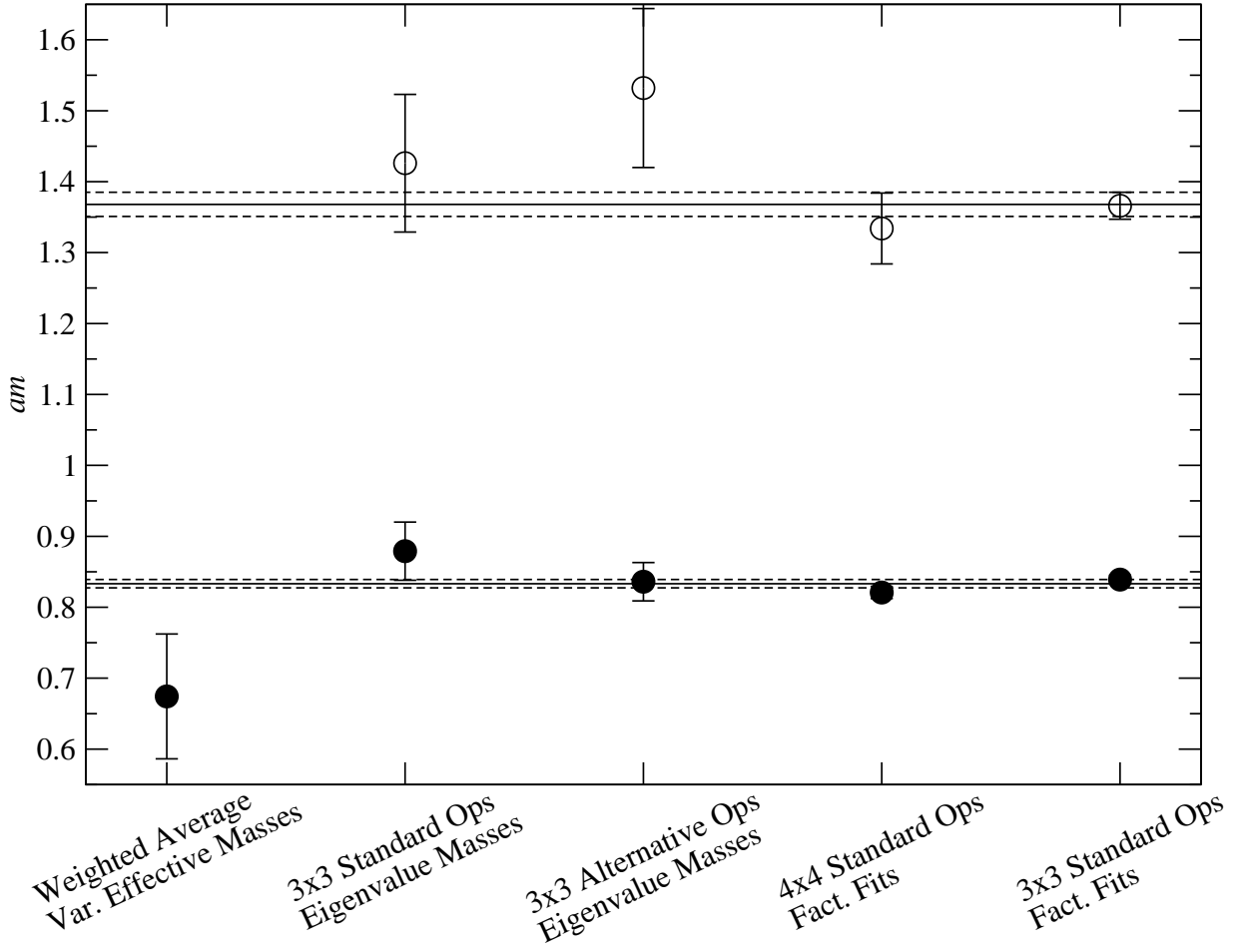


FIG. 12: The overall average for the scalar glueball groundstate mass on the fine ensemble, evaluated as described in the text.

- [34] Particle Data Group, C. Amsler *et al.*, Phys. Lett. **B667**, 1 (2008),
- [35] J. Sexton, A. Vaccarino, and D. Weingarten, Phys. Rev. Lett. **75**, 4563 (1995), hep-lat/9510022,
- [36] M. Chanowitz, Phys. Rev. Lett. **95**, 172001 (2005), hep-ph/0506125,
- [37] L. Lellouch and M. Luscher, Commun. Math. Phys. **219**, 31 (2001), hep-lat/0003023,
- [38] CP-PACS, S. Aoki *et al.*, Phys. Rev. **D76**, 094506 (2007), 0708.3705,
- [39] S. R. Sharpe, R. Gupta, and G. W. Kilcup, Nucl. Phys. **B383**, 309 (1992),
- [40] UKQCD, C. McNeile and C. Michael, Phys. Rev. **D63**, 114503 (2001), hep-lat/0010019,
- [41] S. Miller, *A Study of Glueballs and Scalar Mesons in Lattice QCD*, PhD thesis, University of Liverpool, 2005.
- [42] H.-Y. Cheng, H.-n. Li, and K.-F. Liu, Phys. Rev. **D79**, 014024 (2009), 0811.2577,
- [43] G. Gabadadze, Phys. Rev. **D58**, 055003 (1998), hep-ph/9711380,
- [44] SciDAC, R. G. Edwards and B. Joo, Nucl. Phys. Proc. Suppl. **140**, 832 (2005), hep-lat/0409003,

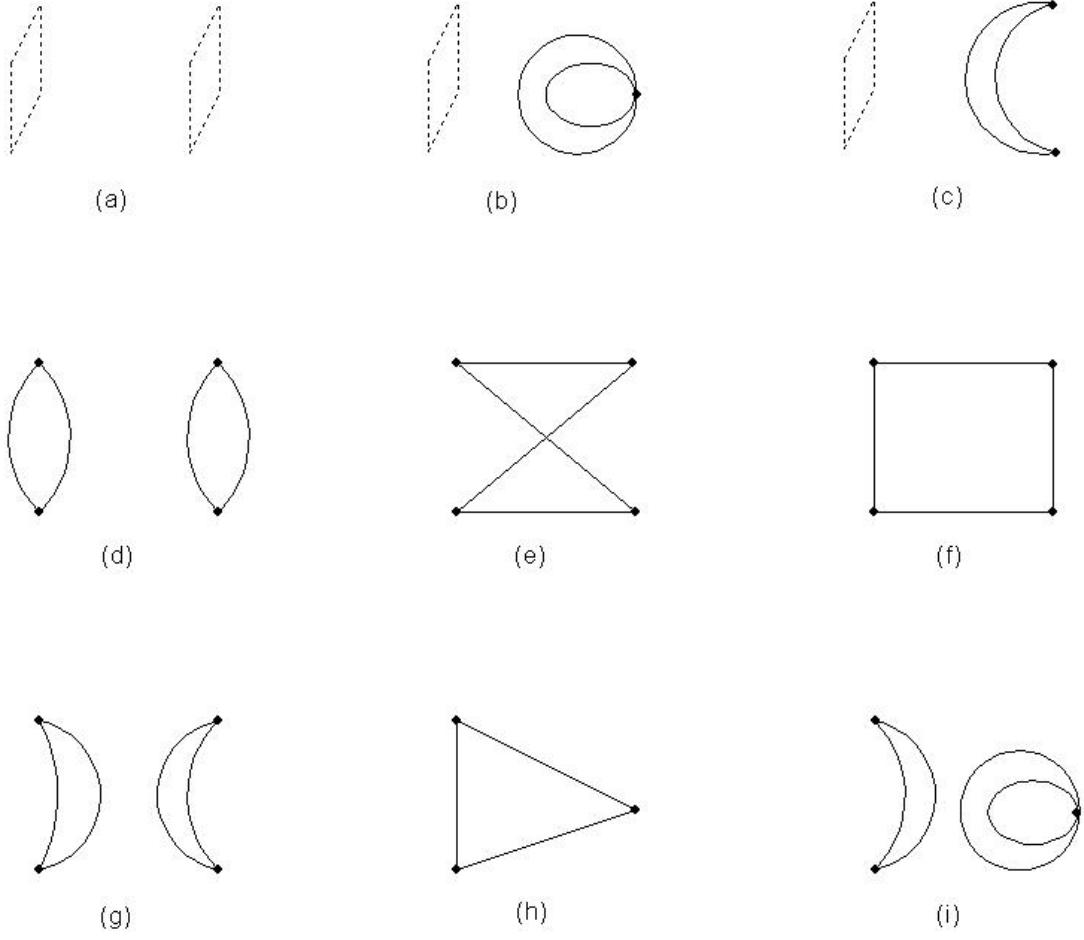


FIG. 13: Schematic mixing diagrams for the full glue, meson, and two meson mixing problem in the $I = 0$ scalar channel. The dashed rectangles represent the glue operators $\mathcal{P}^{A_1^{++}}$ and the solid lines represent quark propagators. Euclidean time runs horizontally.

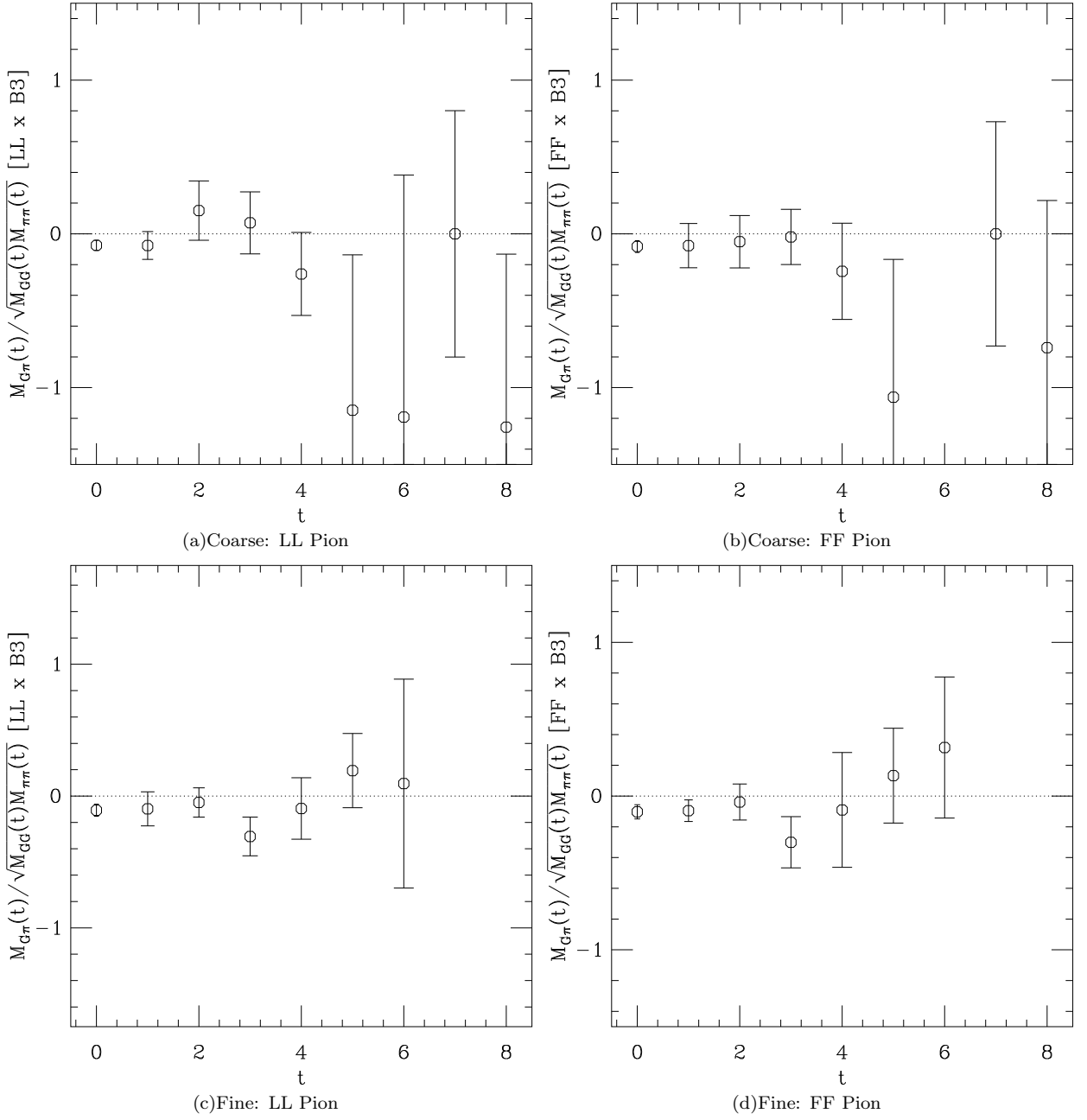


FIG. 14: The measure of glueball- $\pi\pi$ mixing defined in (10) for, clockwise from top-left: the local-local (LL) pion correlators with the three-times Teper blocked glueball operators on the coarse ensemble; the fuzzed-fuzzed (FF) pion correlators with the three-times blocked glueball operators on the coarse ensemble; the fuzzed-fuzzed (FF) pion correlators with the three-times blocked glueball operators on the fine ensemble; and the local-local (LL) pion correlators with the three-times blocked glueball operators on the fine ensemble.

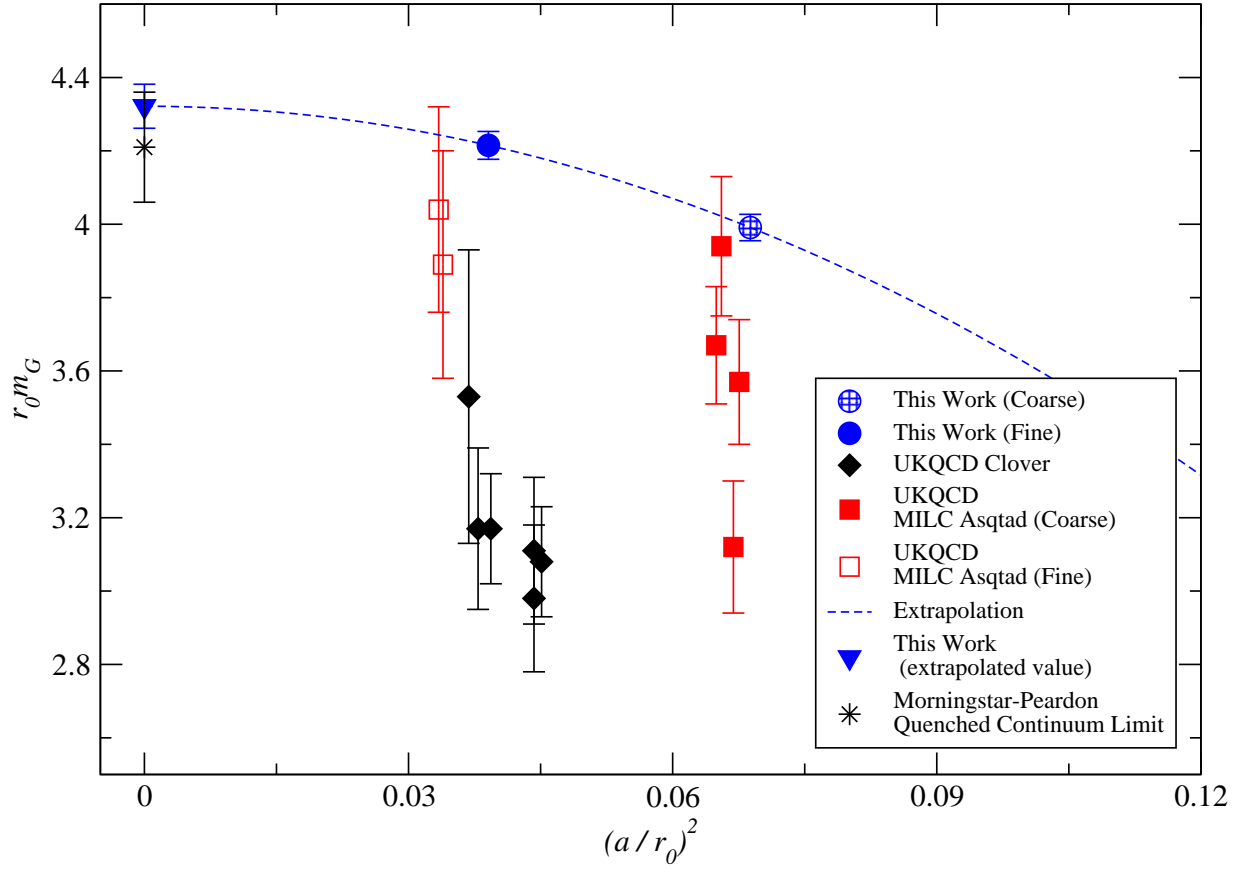


FIG. 15: Our measurements of the scalar glueball mass shown with previous quenched (Morningstar and Peardon [9]) and dynamical (UKQCD on MILC Asqtad [41] and UKQCD Clover [11]) determinations with the continuum extrapolation performed as in [9].

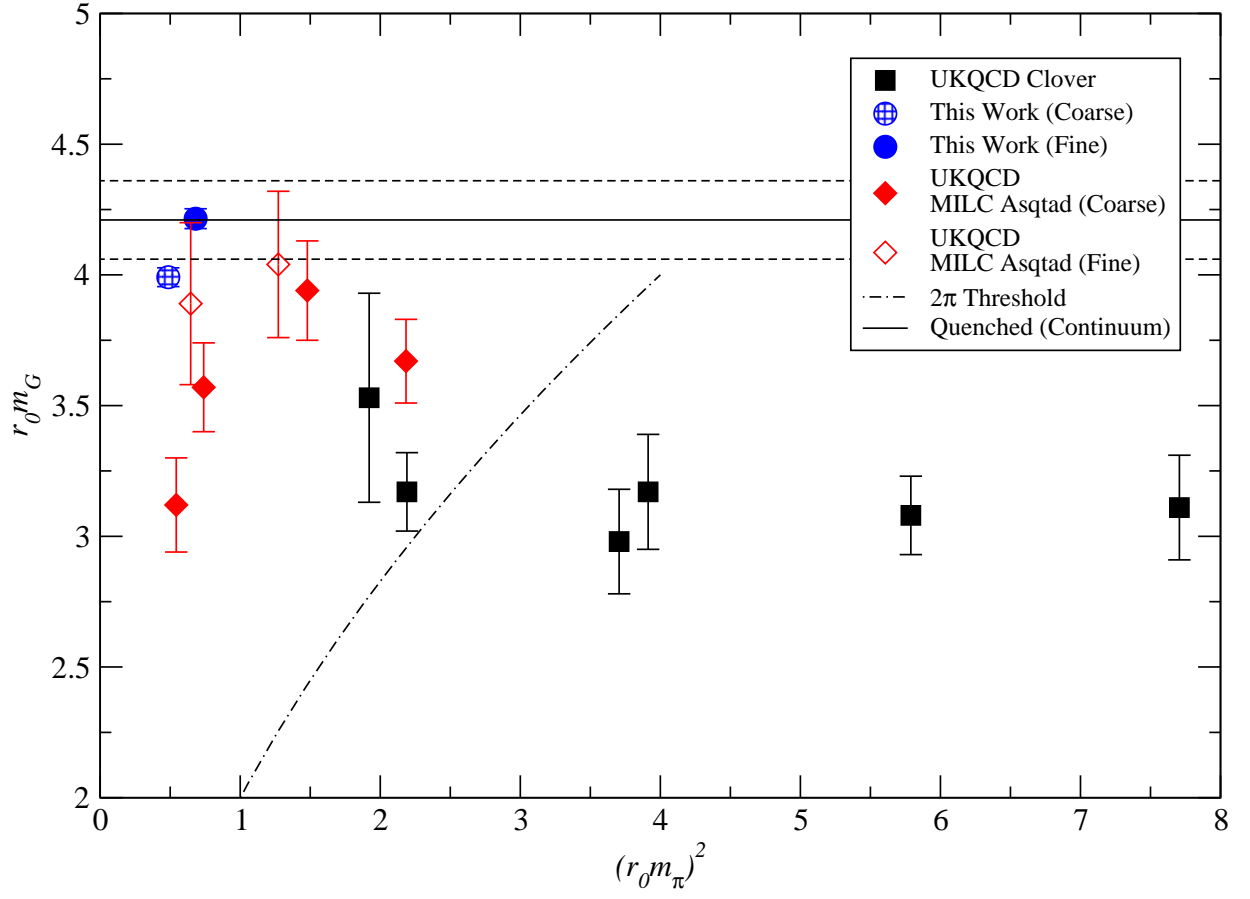


FIG. 16: Our measurements of the scalar glueball mass shown with previous dynamical (UKQCD on MILC Asqtad [41] and UKQCD Clover [11]) determinations. The $\pi\pi$ threshold is shown (dash-dotted line) for convenience.

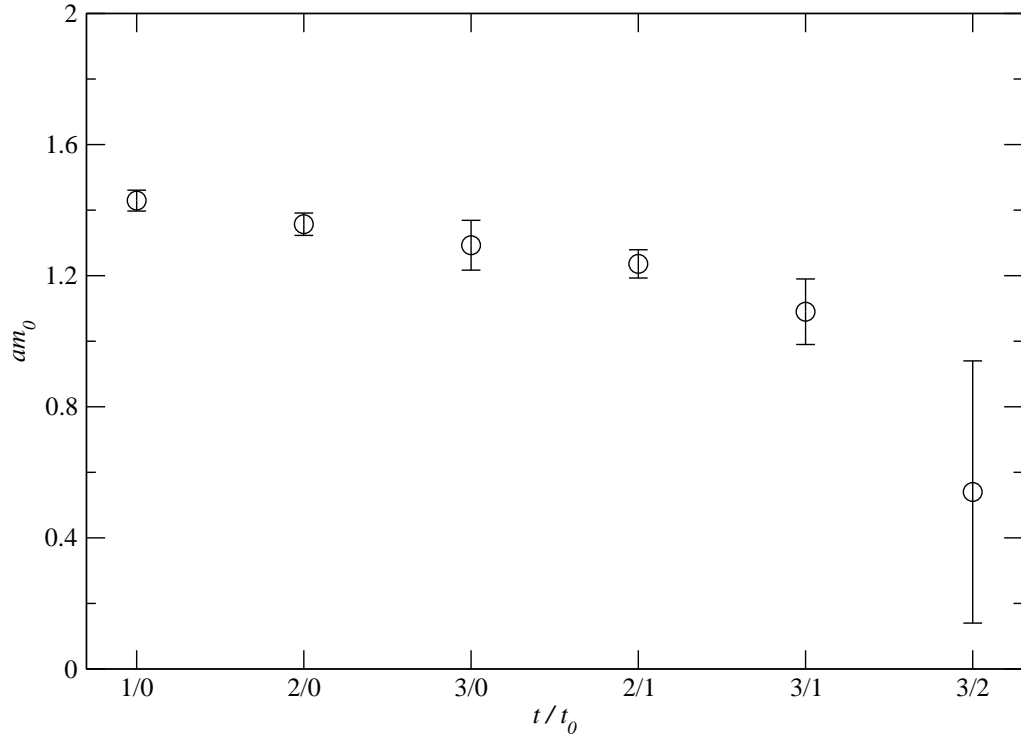


FIG. 17: The masses extracted from the groundstate variational eigenvalues using different t/t_0 projections performed on a 3×3 matrix of correlators formed from the basis of momentum zero pseudoscalar glueball operators $\{\mathcal{H}_0^{A_1^{-+}}, \mathcal{H}_1^{A_1^{-+}}, \mathcal{H}_2^{A_1^{-+}}\}$ on the fine ensemble.

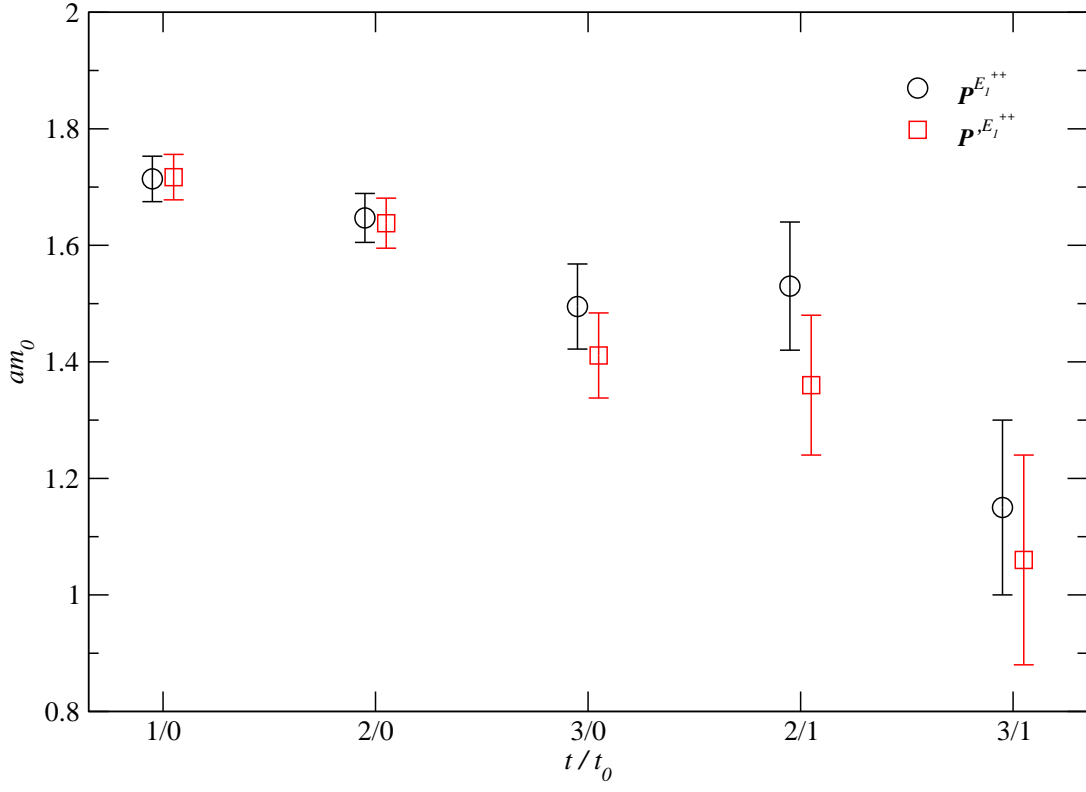


FIG. 18: The masses extracted from the groundstate variational eigenvalues for different t/t_0 projections performed on 4×4 matrices of correlators formed using bases of momentum zero tensor glueball operators $\mathcal{P}^{E_1^{++}}$ (circles) and $\mathcal{P}'^{E_1^{++}}$ (squares) for blocking levels 0, 1, 2 and 3 in each case (coarse ensemble).

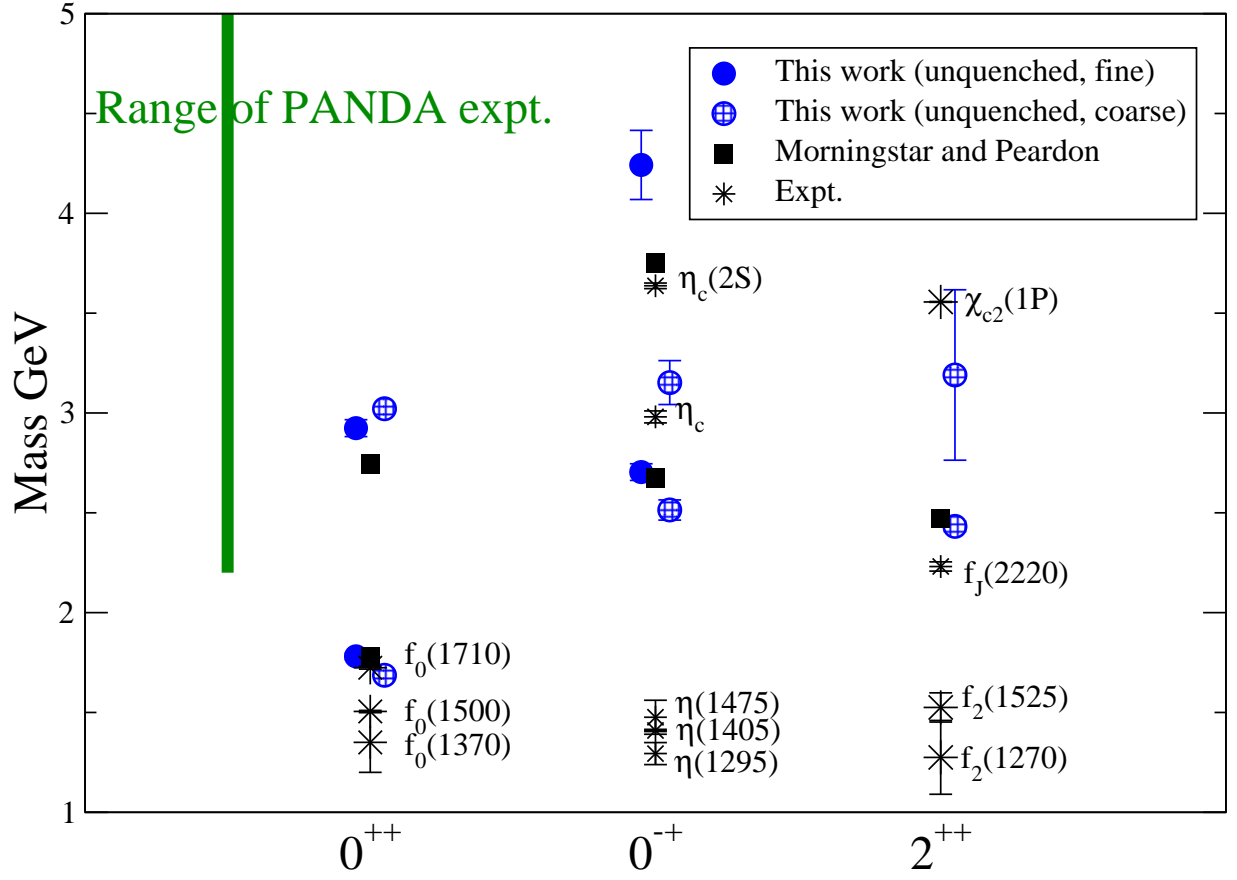


FIG. 19: Comparison of our unquenched glue-sector predictions with experimental states listed in the Particle Data Group listings [34] and with the quenched continuum limit predictions of Morningstar and Peardon [9]. The mass range expected to be investigated in a forthcoming experiment [19] is also indicated